

Deterministic and Universal Frequency-Bin Gate for High-Dimensional Quantum Technologies

Xin Chen*

The College of Electrical and Information Engineering,

Quzhou University, Quzhou 324000, China.

(Dated: December 9, 2025)

Abstract

High-dimensional photonic systems access large Hilbert spaces for quantum information processing. They offer proven advantages in quantum computation, communication, and sensing. However, implementing scalable, low-loss unitary gates across many modes remains a central challenge. Here we propose a deterministic, universal, and fully programmable high-dimensional quantum gate based on a cavity-assisted sum-frequency-generation process, achieving near-unity fidelity. The device implements an $M \times N$ truncated unitary transformation ($1 \leq M < N$), or a full unitary when $M = N$, on frequency-bin modes. With current technology, the attainable dimensionality reaches $M \times N \sim 10^4$, with N up to 10^3 , and can be further increased using multiple pulse shapers. Combined with compatible SPDC sources, high-efficiency detection, and fast feed-forward, this approach provides a scalable, fiber-compatible platform for high-dimensional frequency-bin quantum processing.

Quantum information science has traditionally relied on *qubits*—two-level systems that form the foundation of most existing architectures. Recent advances, however, highlight the benefits of accessing larger Hilbert spaces, either by scaling up the number of qubits or by employing multilevel (d -level) quantum systems (*qudits*) with $d > 2$ [1–3]. Increased dimensionality enables more compact circuit designs [4–7], improves the efficiency of fault-tolerant quantum computation [8–16], enhances communication capacity [17–25], and increases robustness against noise and eavesdropping [26–28]. High-dimensional systems also constitute richer resources for quantum simulation [29–31] and offer advantages in quantum metrology [32–34]. Moreover, high-dimensional states exhibit stronger violations of Bell-type inequalities [35–37].

At the core of high-dimensional quantum technologies lie deterministic, arbitrary multidimensional unitary gates capable of operating with high fidelity. Realizing such gates, however, still requires substantial effort to achieve both scalability and precision. Photons offer a particularly versatile platform: their multiple accessible degrees of freedom—spatial, temporal, and frequency modes—naturally support high-dimensional encodings. Recent demonstrations of high-dimensional quantum gates in both spatial [38, 39] and temporal [40] domains highlight this potential. Nevertheless, these approaches typically require $\sim m^2/2$ two-dimensional gate primitives to synthesize an m -dimensional unitary, demanding many

* chenxin@qzc.edu.cn

optical components together with stringent phase stability and synchronization across large experimental setups. This overhead introduces significant loss and limits achievable fidelity, posing major challenges for further scaling and on-chip integration.

Spectral encoding offers an alternative route to implementing high-dimensional quantum gates. Electro-optic modulator based schemes, combined with pulse shapers, provide reconfigurability and flexibility but rely on active spectral modulation of the quantum field [41–49]. This introduces optical losses and constrains the achievable dimensionality due to the complex temporal waveforms required for radio-frequency driving signals. Another promising approach employs a multi-output quantum pulse gate (QPG) based on dispersion-engineered sum-frequency generation (SFG) processes, enabling programmable frequency-bin interferometers [50–52]. However, these systems are fundamentally limited by the maximal conversion efficiency (CE) of approximately 87.7%, making them intrinsically non-deterministic.

In this work, we propose a deterministic, universal, and fully programmable optical quantum gate for high-dimensional systems based on a cavity-assisted SFG (CSFG) process, achieving near-unity fidelity. The device implements an $M \times N$ truncated unitary transformation ($1 \leq M < N$), or a full unitary when $M = N$, on the input frequency-bin modes. With current state-of-the-art technology, the attainable dimensionality can reach $M \times N \sim 10^4$, and N may extend to 10^3 ; even higher dimensions are feasible by employing multiple pulse shapers. When combined with quantum light sources (both existing and those introduced here), high-efficiency detection, and fast classical feed-forward, this approach provides an efficient and scalable platform for high-dimensional frequency-bin quantum processing, realized within a single fiber-optic spatial mode that offers intrinsic phase stability and compatibility with existing fiber-network infrastructures.

Theoretical model of the quantum gate.— We first implement the $1 \times N$ gate—also known as the QPG [53–57]—and then naturally extend it to the general $M \times N$ case. The $1 \times N$ gate consists of a strong pump pulse, spectrally shaped (via a Fourier-transform pulse shaper) to define the selected gate mode, together with an input signal field. When the signal’s temporal mode (TM) [58, 59] matches that of the pump, the two interact and up-convert the signal into a new idler frequency, whereas orthogonal TMs pass through essentially unchanged. A preliminary $1 \times N$ gate was previously demonstrated in a task-specific protocol [33], targeting a particular TM structure. Here, we develop the general theory and show that the same mechanism enables universal and fully programmable gating. The overall concept is

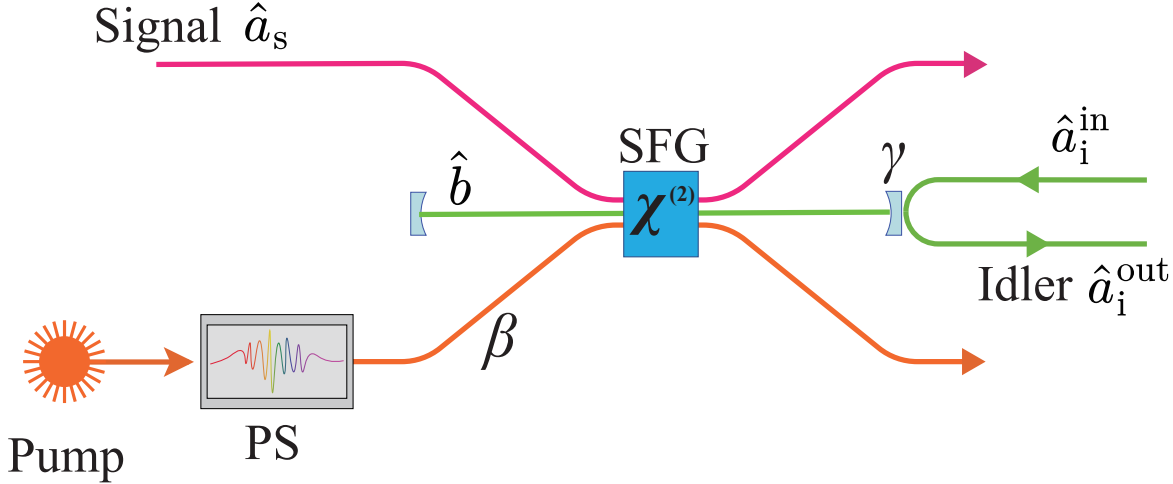


Figure 1. Schematic illustration of the $1 \times N$ gate. PS: pulse shaper.

illustrated in Fig. 1.

All fields are assumed to occupy a single spatial mode (which can be realized using a waveguide) observed within a finite time window T . We take the fields to be one-dimensional and quasi-monochromatic [60]. The strong, undepleted pump pulse has a normalized temporal profile $\beta(t)$, defined such that $\int_{-T/2}^{T/2} |\beta(t)|^2 dt = 1$, and drives a $\chi^{(2)}$ nonlinear medium. In the SFG process, the pump field and the signal field \hat{a}_s interact to generate an idler field at their sum frequency. The idler field is resonantly enhanced by a cavity at frequency $\omega_{i,c}$, with intracavity mode operator \hat{b} coupled to the external field \hat{a}_i . Assuming the pump and signal bandwidths are narrower than the cavity free spectral range (FSR) Ω_{FSR} , only a single resonance contributes. By appropriately choosing the carrier frequencies and polarizations, both energy-conservation and phase-matching conditions are satisfied.

In the rotating frame defined by $\hat{a}_j(\omega_{n_j}) \rightarrow \hat{a}_j(\omega_{n_j})e^{-i\omega_{j,c}t}$, $\hat{b} \rightarrow \hat{b}e^{-i\omega_{i,c}t}$, $\beta(t) \rightarrow \beta(t)e^{-i\omega_{p,c}t}$ where $j \in \{s, i\}$ denotes signal (s) and idler (i) and the carrier frequencies satisfying $\omega_{s,c} + \omega_{p,c} = \omega_{i,c}$, the system Hamiltonian reads

$$\hat{H} = \hat{H}_0 + \hat{H}_1, \quad (1)$$

where $\hat{H}_0/\hbar = \sum_{j,n_j} \omega_{n_j} \hat{a}_j^\dagger(\omega_{n_j}) \hat{a}_j(\omega_{n_j}) + i\sqrt{\gamma}(\hat{a}_i^\dagger \hat{b} - \hat{b}^\dagger \hat{a}_i)$ and $\hat{H}_1/\hbar = -i\eta[\hat{a}_s \hat{b}^\dagger \beta(t) - \hat{a}_s^\dagger \hat{b} \beta^*(t)]$ with $\hat{a}_j = \sqrt{1/T} \sum_{n_j} \hat{a}_j(\omega_{n_j})$, $\omega_{n_j} = n_j \Delta\omega$ and $\Delta\omega = 2\pi/T$. The spatial integrations in the Hamiltonian have already been carried out, and the resulting phase-matching factor in \hat{H}_1 is approximated as a constant—valid for sufficiently narrow pump bandwidths and cavity

linewidths [61]. Here, $\eta > 0$ is the effective nonlinear coupling strength and γ is the cavity decay rate. From Eq. (1), the Heisenberg–Langevin equation for the cavity mode \hat{b} is

$$\dot{\hat{b}}(t) = -\frac{\gamma}{2}\hat{b}(t) - \eta\hat{a}_s^{\text{in}}(t)\beta(t) - \frac{\eta^2}{2}\hat{b}(t)|\beta(t)|^2 - \sqrt{\gamma}\hat{a}_i^{\text{in}}(t), \quad (2)$$

with periodic boundary condition $\hat{b}(T/2) = \hat{b}(-T/2)$. Input/output operators are defined in the time domain as $\hat{a}_j^{\text{in(out)}}(t) = (1/\sqrt{T})\sum_{n_j}\hat{a}_j^{\text{in(out)}}(\omega_{n_j})e^{-i\omega_{n_j}t}$, with $\hat{a}_j^{\text{in(out)}}(\omega_{n_j}) = \hat{a}_j(\omega_{n_j}, \mp T/2)e^{\mp i\omega_{n_j}T/2}$.

Eq. (2) is solved in the frequency domain. Using the input–output boundary condition $a_i^{\text{out}}(t) - a_i^{\text{in}}(t) = \sqrt{\gamma}b(t)$, we obtain an exact expression for the idler output operator at each discrete frequency ω_{n_i} [62]. In the regime $\eta \sim \sqrt{\gamma T} \rightarrow 0$ ($\gamma/\Delta\omega \rightarrow 0$), the output takes the form $\hat{a}_i^{\text{out}}(\omega_0) = \mu'_0\hat{A}_s^{\text{in}}(0) + \nu'_0\hat{a}_i^{\text{in}}(\omega_0)$ and $\hat{a}_i^{\text{out}}(\omega_{n_i}) = \hat{a}_i^{\text{in}}(\omega_{n_i})$ for $n_i \neq 0$, where $\mu'_0 = -2\eta\sqrt{\gamma T}/(\gamma T + \eta^2)$, $|\mu'_0|^2 + |\nu'_0|^2 = 1$, and the TM $\hat{A}_s^{\text{in}}(0) = \sum_{n_s}\beta(\omega_{-n_s})\hat{a}_s^{\text{in}}(\omega_{n_s})$. In particular, when $\eta = \sqrt{\gamma T}$, the output simplifies to

$$\hat{a}_i^{\text{out}}(\omega_{n_i}) = \begin{cases} -\hat{A}_s^{\text{in}}(0), & n_i = 0, \\ \hat{a}_i^{\text{in}}(\omega_{n_i}), & n_i \neq 0, \end{cases} \quad (3)$$

and in this regime both the fidelity and CE approach unity [42, 55]. The fidelity quantifies how closely the implemented transformation matches the ideal one, while the CE gives the probability that the target mode $\hat{A}_s^{\text{in}}(0)$ is successfully converted.

To assess the gate’s performance away from the asymptotic limit, we evaluate its fidelity and CE in the regime of small but nonzero $\gamma/\Delta\omega$. Although the frequency-domain solution of Eq. (2) formally implements an $N \times N$ map on the signal’s frequency-bin modes, the transformation map is highly sparse: only the resonant idler output mode carries appreciable amplitude, so the device operates effectively as a $1 \times N$ gate. In this case, the mapping seen by a single detector becomes measurement-dependent; for instance, photon counting (PC) is sensitive only to the total photon number across all frequency-bin modes and is insensitive to their relative phases. Fig. 2(a) shows the PC-based fidelity and CE of a $1 \times N$ gate for pump spectra given by the second-order Hermite–Gaussian (HG) mode and by a single-frequency-bin (SF) mode [$\beta(t) = 1/\sqrt{T}$], plotted versus $\gamma/\Delta\omega$ under the constraint $\eta = \sqrt{\gamma T}$. The SF-mode fidelity is lower than the HG-mode fidelity: HG modes vary smoothly in frequency, so adjacent bins have nearly identical amplitudes, allowing high fidelity even when the gate does not sharply resolve individual pump-frequency bins. In contrast, the SF-mode fidelity

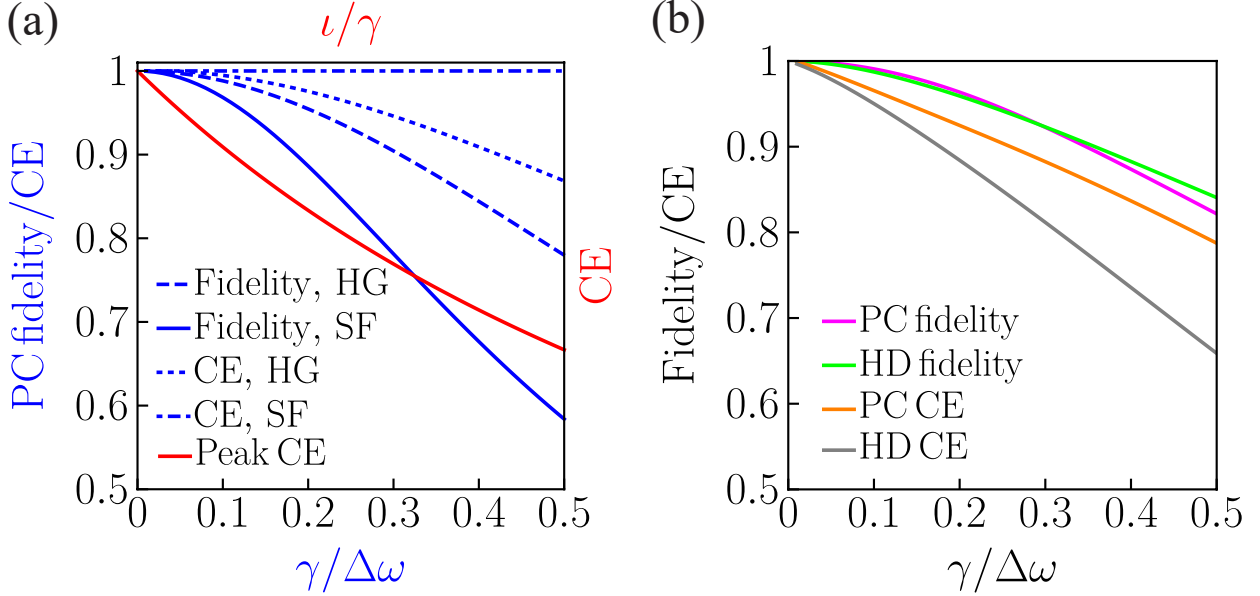


Figure 2. Fidelity and CE of the quantum gate. (a) PC fidelity and CE of the effective $1 \times N$ gate versus $\gamma/\Delta\omega$, evaluated under the condition $\eta = \sqrt{\gamma T}$, for a second-order HG pump and an SF pump $\beta(t) = 1/\sqrt{T}$. The red curve shows the peak achievable CE as a function of ι/γ in the limit $\eta = \sqrt{(\gamma + \iota)T} \rightarrow 0$. (b) PC and HD fidelities, together with the corresponding CE, for a 101×101 gate versus $\gamma/\Delta\omega$, evaluated with respect to the ideal identity transformation under $\eta = \sqrt{\gamma T}$, using the pump $\beta(t) = -(1/\sqrt{T}) \sum_m e^{-i(\omega_{p,c,m} - m\Delta\omega)t}$.

more stringently reflects the limit of the gate. The SF-mode CE is unity, as follows from the solution of Eq. (2) with the flat pump intensity $|\beta(t)|^2 = 1/T$ [62]. Finally, because homodyne detection (HD) already performs a $1 \times N$ mode-selection operation, applying it after another $1 \times N$ gate is redundant, and we therefore omit HD-based fidelity analysis here.

To incorporate internal losses, we model coupling to an ancillary bath mode \hat{d}^{in} with loss rate ι . In the limit $\eta \sim \sqrt{(\gamma + \iota)T} \rightarrow 0$, the idler output in the frequency domain becomes $\hat{a}_i^{\text{out}}(\omega_0) = \mu_0'' \hat{A}_s^{\text{in}}(0) + \nu_0'' \hat{a}_i^{\text{in}}(\omega_0) + v_0'' \hat{d}^{\text{in}}(\omega_0)$ and $\hat{a}_i^{\text{out}}(\omega_{n_i}) = \hat{a}_i^{\text{in}}(\omega_{n_i})$ for $n_i \neq 0$, where $\mu_0'' = -2\eta\sqrt{\gamma T}/(\gamma T + \iota T + \eta^2)$ and the normalization condition $|\mu_0''|^2 + |\nu_0''|^2 + |v_0''|^2 = 1$ ensures unitarity [62]. The CE, given by $|\mu_0''|^2$, reaches its maximum value $1/(1 + \iota/\gamma)$ at $\eta = \sqrt{(\gamma + \iota)T}$, as shown in Fig. 2(a), indicating that internal losses reduce the achievable peak CE. An ideal deterministic gate requires $\iota = 0$, whereas in practice a near-deterministic gate can be realized when the relative internal-loss ratio ι/γ is sufficiently small.

The $1 \times N$ quantum gate based on the CSFG naturally extends to an $M \times N$ gate. Let the cavity resonances be $\omega_{i,c,m} = \omega_{i,c} + m\Omega_{\text{FSR}}$, and denote the corresponding idler modes by $\hat{a}_{i,m}$, each with bandwidth smaller than Ω_{FSR} . The signal field \hat{a}_s is assumed to have the same bandwidth. The pump field is taken as $\beta(t) = \sum_m \beta_m(t) e^{-i\omega_{p,c,m}t}$, where each tone $\beta_m(t) e^{-i\omega_{p,c,m}t}$ has a bandwidth matched to the signal and idler fields and is centered at $\omega_{p,c,m} = \omega_{p,c} + m\Omega_{\text{FSR}}$. The pump envelopes $\{\beta_m(t)\}$ are mutually orthogonal, allowing the dynamics to decompose into independent resonance channels in the limit $\eta = \sqrt{\gamma T} \rightarrow 0$ ($\gamma/\Delta\omega \rightarrow 0$) [62]. In this regime, the idler output at each resonance becomes $\hat{a}_{i,m}^{\text{out}}(\omega_0) = -\hat{A}_{s,m}^{\text{in}}(0)$ and $\hat{a}_{i,m}^{\text{out}}(\omega_{n_i}) = \hat{a}_{i,m}^{\text{in}}(\omega_{n_i})$ for $n_i \neq 0$, where $\hat{A}_{s,m}^{\text{in}}(0) = \sum_{n_s} \beta_m(\omega_{-n_s}) \hat{a}_s^{\text{in}}(\omega_{n_s})$. This implements an $M \times N$ truncated-unitary transformation (unitary when $M = N$) on the frequency-bin modes [51], yielding the idler output

$$\hat{a}_{i,m}^{\text{out}}(\omega_0) = \sum_l U_{ml} \hat{a}_s^{\text{in}}(\omega_l), \quad (4)$$

where $U_{ml} = -\beta_m(\omega_{-l})$.

Each idler channel of the $M \times N$ gate can be measured via PC or HD following wavelength-division demultiplexing (WDD). Fig. 2(b) shows the PC and HD fidelities, together with the corresponding CE, for a 101×101 gate as functions of $\gamma/\Delta\omega$, evaluated with respect to the ideal identity transformation. The results are obtained using the pump field $\beta(t) = -(1/\sqrt{T}) \sum_m e^{-i(\omega_{p,c,m} - m\Delta\omega)t}$. When placed before the WDD, this identity gate can enable effective demultiplexing at denser channel spacings. Because HD projects each output channel onto a single TM and discards all orthogonal modes, it is sensitive to mode-mismatch loss, and its CE is therefore typically lower than the PC-based CE.

Schemes for high-dimensional quantum processing.— Combined with nonclassical sources, measurement, and fast feed-forward, the quantum gate provides a scalable platform for high-dimensional frequency-bin quantum processing, supporting applications in quantum computation, simulation, communication, and sensing. We outline several representative schemes below.

A continuous-wave pump with linewidth $\ll \Delta\omega$ drives spontaneous parametric down-conversion (SPDC) within the observation window T , naturally generating nonclassical states in discrete frequency-bin modes that are directly compatible with the gate [33]. A nondegenerate SPDC source yields M entangled signal–idler mode pairs in two-mode squeezed-vacuum (TMSV) states with uniform squeezing across modes, while a degenerate

source generates M single-mode squeezed-vacuum (SMSV) states with identical squeezing. The nondegenerate source additionally enables heralded single photons distributed over M frequency bins. An alternative source is SPDC in a nonlinear resonator, which produces analogous squeezed, entangled, or heralded single-photon states directly in frequency-comb-bin modes [63–65]. Note that while we focus on SPDC, the same formalism applies to stimulated parametric down-conversion, yielding displaced squeezed states; this is optional for the schemes considered below.

Fig. 3(a) shows a scheme in which the signal modes of N entangled pairs pass through a phase-shifted thermal-loss channel (e.g., target reflection or information encoding) and are then heterodyne-detected. The heterodyne outcomes are used to program a $1 \times N$ gate acting on the idler modes, followed by PC. This realizes the correlation-to-displacement conversion protocol, enabling near-optimal performance in quantum illumination, phase sensing, and communication [33, 34, 66–68]. Fig. 3(b) depicts a scheme in which M ($M \leq N$) input SMSV states are processed by a fully programmable $N \times N$ gate, followed by HD or PC. This architecture underlies applications such as Gaussian boson sampling [30] and measurement-based continuous-variable quantum computation [14, 15]. The programmable $N \times N$ gate also operates at the single-photon level, e.g., as a high-dimensional Bell-state analyzer that enables entanglement swapping between remote matter qudits and boosts entanglement distribution rates by exploiting enlarged mode dimensionality [69–72]. Fig. 3(c) shows a programmable heralded multimode single-photon (qudit) source, obtained by heralding the signal output of a nondegenerate SPDC source after spectral mode selection by a $1 \times N$ gate. The resulting qudit state can be directly interfaced with the $N \times N$ gate for applications such as high-dimensional quantum key distribution [26, 73]. Fig. 3(d) shows the generation of M ($M \leq N$) independent single-photon sources, $\bigotimes_{n=-(M-1)/2}^{(M-1)/2} |1\rangle_n$, each occupying a distinct frequency-bin mode, by coincident heralding of all signal modes of the nondegenerate SPDC source (for WDD with denser channel spacing, a previously discussed $M \times M$ identity gate may be used to enhance channel separation). Combined with the programmable $N \times N$ gate, this configuration provides a universal resource for high-dimensional photonic quantum computation [39, 74, 75].

Scaling.— The dimensionality of the quantum gate is primarily limited by the nonlinear interaction bandwidth and the spectral resolution of the pump shaper. Although SFG can in principle support bandwidths of 1–10 THz [76], faithful mode mapping requires the phase-

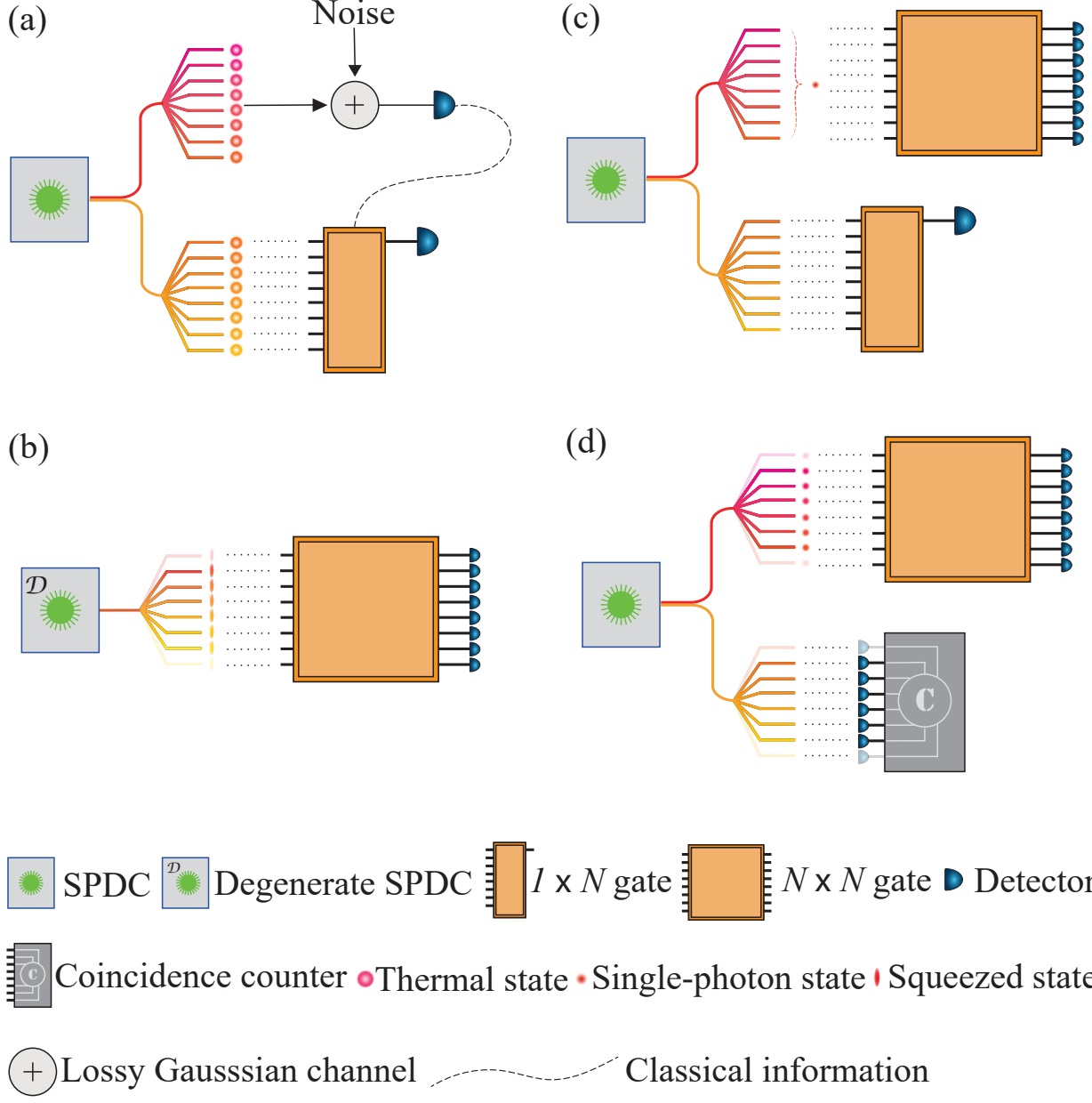


Figure 3. Representative schemes for high-dimensional quantum processing using the programmable frequency-bin gate.

matching response to remain flat across the pump bandwidth (so that the pump spectrum maps to the converted TM without distortion), reducing the usable signal bandwidth to $\Omega_s \sim 0.1\text{--}1$ THz [33, 61]. Taking $\Omega_s = 1$ THz and a commercial Fourier-transform pulse shaper with resolution $R \sim 1$ GHz yields $N = \Omega_s/R \sim 10^3$ accessible frequency bins. For an $M \times N$ gate, the total dimensionality is further limited by the programmable bandwidth of the shaper, which currently supports on the order of $M \times N \sim 10^4$ modes. The di-

mensionality can be further extended by employing multiple pulse shapers. While cavity parameters (linewidth and FSR) affect the gate—high fidelity and CE require $\gamma/\Delta\omega \lesssim 0.01$ and $\iota/\gamma \lesssim 0.01$ (Fig. 2), and the FSR bounds the usable signal bandwidth—current resonator technology (sub-MHz linewidths and finesse up to 10^6) readily accommodates the dimensionalities considered here.

On the source side, an SPDC process pumped by a narrow-linewidth continuous-wave laser serves as the time-reversed analog of CSFG, so its phase-matching bandwidth naturally matches the mode-bandwidth requirement of the $M \times N$ gate. Although the pump linewidth can, in principle, influence fidelity and scalability of the system [51], modern single-frequency lasers provide ultranarrow linewidths [77], so the photon source does not impose a practical scalability constraint.

Conclusion.— We have demonstrated that cavity-assisted SFG enables deterministic, programmable, and high-fidelity quantum gates across exceptionally large frequency-bin Hilbert spaces. Under realistic parameters, the scheme supports 10^2 – 10^3 spectral modes within a single fiber-guided spatial mode, providing intrinsic phase stability and compatibility with telecom-band quantum sources. These capabilities make the gate a practical and scalable resource for high-dimensional photonic quantum processors, quantum networks, and measurement-based quantum protocols.

Appendix A: Detailed analysis of the $1 \times N$ gate

In this section, we present a detailed analysis of the $1 \times N$ gate based on the CSFG process. The total Hamiltonian reads

$$\hat{H}/\hbar = \omega_{i,c} \hat{b}^\dagger \hat{b} + \sum_{j,n_j} [(\omega_{n_j} + \omega_{j,c}) \hat{a}_j^\dagger(\omega_{n_j}) \hat{a}_j(\omega_{n_j})] + i\sqrt{\gamma} (\hat{a}_i^\dagger \hat{b} - \hat{b}^\dagger \hat{a}_i) - i\eta [\hat{a}_s \hat{b}^\dagger \beta(t) - \hat{a}_s^\dagger \hat{b} \beta^*(t)]. \quad (A1)$$

Here \hat{a}_s denotes the signal mode, \hat{b} the intracavity idler mode with central frequency $\omega_{i,c}$, and \hat{a}_i the external idler field coupled to the cavity. The pump envelope $\beta(t)$ is normalized such that $\int_{-T/2}^{T/2} |\beta(t)|^2 dt = 1$. The mode operators are defined as $\hat{a}_j = \sqrt{1/T} \sum_{n_j} \hat{a}_j(\omega_{n_j})$, where $\omega_{n_j} = n_j \Delta\omega$ and $\Delta\omega = 2\pi/T$, with $j \in \{s, i\}$ labeling the signal and idler fields. Transforming to the rotating frame $\hat{a}_j(\omega_{n_j}) \rightarrow \hat{a}_j(\omega_{n_j}) e^{-i\omega_{j,c}t}$, $\hat{b} \rightarrow \hat{b} e^{-i\omega_{i,c}t}$, $\beta(t) \rightarrow \beta(t) e^{-i\omega_{p,c}t}$ with

$\omega_{s,c} + \omega_{p,c} = \omega_{i,c}$, the Hamiltonian simplifies to

$$\hat{H} = \hat{H}_0 + \hat{H}_1, \quad (\text{A2})$$

where $\hat{H}_0/\hbar = \sum_{j,n_j} \omega_{n_j} \hat{a}_j^\dagger(\omega_{n_j}) \hat{a}_j(\omega_{n_j}) + i\sqrt{\gamma}(\hat{a}_i^\dagger \hat{b} - \hat{b}^\dagger \hat{a}_i)$ and $\hat{H}_1/\hbar = -i\eta[\hat{a}_s \hat{b}^\dagger \beta(t) - \hat{a}_s^\dagger \hat{b} \beta^*(t)]$.

a. *Remark.* The spatial integrals in the nonlinear-interaction Hamiltonian have already been carried out. In \hat{H}_1 , the phase-matching factor $C = \int_0^L e^{i\Delta kz} dz$ is treated as a constant. This approximation is justified because the cavity linewidth and pump bandwidth are chosen such that only frequency components satisfying $\Delta k L \ll 1$ experience appreciable gain, while off-phase-matched components are strongly suppressed. Here $\Delta k = k_i - k_s - k_p$ is the phase mismatch, with k_s, k_p, k_i the signal, pump, and idler wavevectors, and L the nonlinear-interaction length [33].

Furthermore, the cavity FSR is chosen to exceed the pump bandwidth, ensuring that only a single cavity resonance participates in the conversion process.

From Eq. (A2), the Heisenberg equations of motion for $\hat{a}_j(\omega_{n_j})$ and \hat{b} are

$$\dot{\hat{a}}_s(\omega_{n_s}, t) = -i\omega_{n_s} \hat{a}_s(\omega_{n_s}, t) + \frac{\eta}{\sqrt{T}} \hat{b}(t) \beta^*(t), \quad (\text{A3})$$

$$\dot{\hat{a}}_i(\omega_{n_i}, t) = -i\omega_{n_i} \hat{a}_i(\omega_{n_i}, t) + \sqrt{\frac{\gamma}{T}} \hat{b}(t), \quad (\text{A4})$$

$$\dot{\hat{b}}(t) = -\eta \hat{a}_s(t) \beta(t) - \sqrt{\gamma} \hat{a}_i(t). \quad (\text{A5})$$

Solving Eqs. (A3)–(A4) following the method of Ref. [78] gives

$$\hat{a}_s(\omega_{n_s}, t) = e^{-i\omega_{n_s}(t+T/2)} \hat{a}_s(\omega_{n_s}, -T/2) + \frac{\eta}{\sqrt{T}} \int_{-T/2}^t e^{-i\omega_{n_s}(t-t')} \hat{b}(t') \beta^*(t') dt', \quad (\text{A6})$$

$$\hat{a}_i(\omega_{n_i}, t) = e^{-i\omega_{n_i}(t+T/2)} \hat{a}_i(\omega_{n_i}, -T/2) + \sqrt{\frac{\gamma}{T}} \int_{-T/2}^t e^{-i\omega_{n_i}(t-t')} \hat{b}(t') dt'. \quad (\text{A7})$$

Thus,

$$\hat{a}_s(t) = \frac{1}{\sqrt{T}} \sum_{n_s} \hat{a}_s(\omega_{n_s}, t) = \hat{a}_s^{\text{in}}(t) + \frac{\eta}{2} \hat{b}(t) \beta^*(t), \quad (\text{A8})$$

$$\hat{a}_i(t) = \frac{1}{\sqrt{T}} \sum_{n_i} \hat{a}_i(\omega_{n_i}, t) = \hat{a}_i^{\text{in}}(t) + \frac{\sqrt{\gamma}}{2} \hat{b}(t). \quad (\text{A9})$$

Here, the input/output operators $\hat{a}_j^{\text{in}(\text{out})}(t) = (1/\sqrt{T}) \sum_{n_j} \hat{a}_j^{\text{in}(\text{out})}(\omega_{n_j}) e^{-i\omega_{n_j}t}$, with $\hat{a}_j^{\text{in}(\text{out})}(\omega_{n_j}) = \hat{a}_j(\omega_{n_j}, \mp T/2) e^{\mp i\omega_{n_j}T/2}$ as defined in the main text. Substituting Eqs. (A8)–(A9) into Eq. (A5) yields the Langevin equation for the cavity mode:

$$\dot{\hat{b}}(t) = -\frac{\gamma}{2} \hat{b}(t) - \eta \hat{a}_s^{\text{in}}(t) \beta(t) - \frac{\eta^2}{2} \hat{b}(t) |\beta(t)|^2 - \sqrt{\gamma} \hat{a}_i^{\text{in}}(t), \quad (\text{A10})$$

subject to the periodic boundary condition $\hat{b}(T/2) = \hat{b}(-T/2)$. The solution has the form

$$\hat{b}(t) = \sum_j \int_{-T/2}^{T/2} g'_j(t, t') \hat{a}_j^{\text{in}}(t') dt', \quad (\text{A11})$$

where the kernels are

$$g'_j(t, t') = - \left[\frac{e^{-\gamma T/2 - \eta^2/2}}{1 - e^{-\gamma T/2 - \eta^2/2}} + \Theta(t - t') \right] h_j(t') \exp \left[- \int_{t'}^t \left(\frac{\gamma}{2} + \frac{\eta^2}{2} |\beta(t'')|^2 \right) dt'' \right], \quad (\text{A12})$$

with $h_s(t) = \eta \beta(t)$, $h_i(t) = \sqrt{\gamma}$ and Θ the Heaviside step function. Using the cavity input–output relation

$$\hat{a}_i^{\text{out}}(t) - \hat{a}_i^{\text{in}}(t) = \sqrt{\gamma} \hat{b}(t), \quad (\text{A13})$$

together with Eq. (A11), the idler output operator can be written directly as

$$\hat{a}_i^{\text{out}}(t) = \sum_j \int_{-T/2}^{T/2} g_j(t, t') \hat{a}_j^{\text{in}}(t') dt', \quad (\text{A14})$$

where $g_s(t, t') = \sqrt{\gamma} g'_s(t, t')$ and $g_i(t, t') = \sqrt{\gamma} g'_i(t, t') + \delta(t, t')$.

To access the operating regime of interest, we consider the limit $\eta \sim \sqrt{\gamma T} \rightarrow 0$ ($\gamma/\Delta\omega \rightarrow 0$). In this regime, Eq. (A12) reduces to

$$g'_j(t, t') = -2h_j(t')/(\gamma T + \eta^2). \quad (\text{A15})$$

Consequently, the intracavity field becomes

$$\hat{b}(t) = - \int_{-T/2}^{T/2} \frac{2}{\gamma T + \eta^2} [\eta \beta(t') \hat{a}_s^{\text{in}}(t') + \sqrt{\gamma} \hat{a}_i^{\text{in}}(t')] dt' \quad (\text{A16})$$

$$= -\frac{2}{\gamma T + \eta^2} [\eta \hat{A}_s^{\text{in}}(0) + \sqrt{\gamma T} \hat{a}_i^{\text{in}}(\omega_0)], \quad (\text{A17})$$

where the TM $\hat{A}_s^{\text{in}}(n_i) = \sum_{n_s} \beta(\omega_{n_i - n_s}) \hat{a}_s^{\text{in}}(\omega_{n_s})$. In the frequency domain,

$$\hat{b}(\omega_{n_i}) = \begin{cases} -\frac{2}{\gamma T + \eta^2} [\eta \sqrt{T} \hat{A}_s^{\text{in}}(0) + \sqrt{\gamma T} \hat{a}_i^{\text{in}}(\omega_0)], & n_i = 0, \\ 0, & n_i \neq 0. \end{cases} \quad (\text{A18})$$

The idler output field follows as

$$\hat{a}_i^{\text{out}}(\omega_{n_i}) = \begin{cases} -\frac{1}{\gamma T + \eta^2} [2\eta \sqrt{\gamma T} \hat{A}_s^{\text{in}}(0) + (\gamma T - \eta^2) \hat{a}_i^{\text{in}}(\omega_0)], & n_i = 0, \\ \hat{a}_i^{\text{in}}(\omega_{n_i}), & n_i \neq 0. \end{cases} \quad (\text{A19})$$

In particular, when $\eta = \sqrt{\gamma T}$, the output reduces to

$$\hat{a}_i^{\text{out}}(\omega_{n_i}) = \begin{cases} -\hat{A}_s^{\text{in}}(0), & n_i = 0, \\ \hat{a}_i^{\text{in}}(\omega_{n_i}), & n_i \neq 0. \end{cases} \quad (\text{A20})$$

1. Transfer function

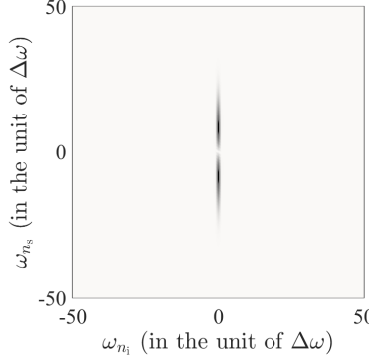


Figure 4. Amplitude of the frequency-domain transfer function $\tilde{g}_s(\omega_{n_i}, \omega_{m_s})$ for the CSFG process. Parameters: $\gamma/\Delta\omega = \eta^2/2\pi = 10^{-2}$. For numerical tractability, the calculation uses 101 discrete frequency-bin modes, with the pump field encoded in the second-order HG mode.

To illustrate the frequency decorrelation between the signal and idler fields, Fig. 4 plots the amplitude of the frequency-domain transfer function. The transfer function is defined as [55]

$$\tilde{g}_s(\omega_{n_i}, \omega_{m_s}) = \frac{1}{T} \int_{-T/2}^{T/2} dt \int_{-T/2}^{T/2} dt' e^{i\omega_{n_i} t} g_s(t, t') e^{-i\omega_{m_s} t'}. \quad (\text{A21})$$

The calculation is performed in the parameter regime of interest, where $\gamma/\Delta\omega = \eta^2/2\pi = 10^{-2}$.

2. Fidelity and conversion efficiency

In the regime of small but nonzero $\gamma/\Delta\omega$, the frequency-domain solution of Eq. (A10) formally implements an $N \times N$ transformation on the input signal's frequency-bin modes. However, the resulting map \tilde{g}_s is highly sparse: only the resonant output mode carries appreciable amplitude. The device therefore operates effectively as a $1 \times N$ gate. At first glance, one might assess its performance by comparing the full $N \times N$ map \tilde{g}_s to the ideal transformation. In practice, however, the device is used as a $1 \times N$ gate monitored by a single detector, so the effective transformation seen by the detector is measurement dependent, and the corresponding detection-associated fidelity is the appropriate figure of merit for the application. For example, a photon counter with limited spectral resolution measures only the total photon number across all output modes. In this situation the measurement corresponds to

$$\hat{n} = \int_{-T/2}^{T/2} dt \hat{a}_i^{\text{out}\dagger}(t) \hat{a}_i^{\text{out}}(t) = \int_{-T/2}^{T/2} du du' \hat{a}_s^{\text{in}\dagger}(u) \mathcal{U}(u, u') \hat{a}_s^{\text{in}}(u'),$$

where the associated kernel is

$$\mathcal{U}(u, u') = \int_{-T/2}^{T/2} dt g_s^*(t, u) g_s(t, u'). \quad (\text{A22})$$

Although the idler input modes are formally included in Eq. (A14), we retain only the converted-mode contribution and omit the trivial vacuum terms here.

Since \mathcal{U} is Hermitian and positive semidefinite by construction, we may regard $\rho = \mathcal{U}/(\text{Tr } \mathcal{U})$ as an effective density matrix. For the ideal transformation in the time domain, $g_s^{\text{ideal}}(t, u) \propto \beta(u)$, the corresponding kernel is $\mathcal{U}^{\text{ideal}}(u, u') = \beta^*(u)\beta(u')$, whose normalized form $\sigma = \mathcal{U}^{\text{ideal}}/(\text{Tr } \mathcal{U}^{\text{ideal}})$ represents a pure state. Borrowing the standard quantum-state fidelity, we define the PC fidelity as

$$\mathcal{F}_i^{\text{PC}} = \text{Tr}(\rho\sigma) = \frac{\text{Tr}(\mathcal{U}\mathcal{U}^{\text{ideal}})}{(\text{Tr } \mathcal{U})(\text{Tr } \mathcal{U}^{\text{ideal}})} = \frac{\int_{-T/2}^{T/2} dt \left| \int_{-T/2}^{T/2} du g_s(t, u) \beta^*(u) \right|^2}{\int_{-T/2}^{T/2} \int_{-T/2}^{T/2} dt du |g_s(t, u)|^2}, \quad (\text{A23})$$

where we have used $\int_{-T/2}^{T/2} du |\beta(u)|^2 = 1$. Correspondingly, the CE—the probability that the target mode $\hat{A}_s^{\text{in}}(0)$ is successfully converted—is

$$\mathcal{C}_e^{\text{PC}} = \frac{\text{Tr}(\mathcal{U}\mathcal{U}^{\text{ideal}})}{(\text{Tr } \mathcal{U}^{\text{ideal}})^2} = \int_{-T/2}^{T/2} dt \left| \int_{-T/2}^{T/2} du g_s(t, u) \beta^*(u) \right|^2. \quad (\text{A24})$$

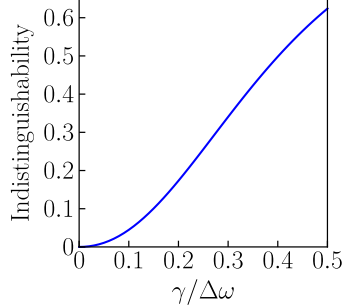


Figure 5. Indistinguishability of $1 \times N$ gate outputs for pumps in adjacent SF modes versus $\gamma/\Delta\omega$, evaluated under the condition $\eta = \sqrt{\gamma T}$.

Finally, because HD already performs a $1 \times N$ mode-selection by itself, applying it after another $1 \times N$ gate is redundant, and we therefore omit HD fidelity analysis here.

3. Control-mode spectral sensitivity

To complement the fidelity analysis, we investigate the gate's ability to distinguish the outputs produced by pump fields in two adjacent SF modes, assessed via PC. We encode the pump field in two TMs, $\beta(t) = (1/\sqrt{T})e^{-i\omega_n t}$ and $(1/\sqrt{T})e^{-i\omega_{n+1} t}$, corresponding to two nearby SF modes at ω_n and ω_{n+1} . Since $|\beta(t)|^2 = 1/T$ for both cases, solving Eq. (A10) in the frequency domain yields

$$\hat{b}(\omega_{n_i}) = \frac{\frac{\eta}{\sqrt{T}}}{i\omega_{n_i} - \frac{\gamma}{2} - \frac{\eta^2}{2T}} \hat{A}_s^{\text{in}}(n_i) + \frac{\sqrt{\gamma}}{i\omega_{n_i} - \frac{\gamma}{2} - \frac{\eta^2}{2T}} \hat{a}_i^{\text{in}}(\omega_{n_i}), \quad (\text{A25})$$

where $\hat{A}_s^{\text{in}}(n_i) = \hat{a}_s^{\text{in}}(\omega_{n_i-n})$ and $\hat{a}_s^{\text{in}}(\omega_{n_i-n-1})$ for the two pump configurations, respectively. Using the cavity input-output relation

$$\hat{a}_i^{\text{out}}(t) - \hat{a}_i^{\text{in}}(t) = \sqrt{\gamma} \hat{b}(t), \quad (\text{A26})$$

we obtain

$$\hat{a}_i^{\text{out}}(\omega_{n_i}) = \mu'_{n_i} \hat{A}_s^{\text{in}}(n_i) + \nu'_{n_i} \hat{a}_i^{\text{in}}(\omega_{n_i}), \quad (\text{A27})$$

where

$$\mu'_{n_i} = \frac{\eta \sqrt{\gamma/T}}{i\omega_{n_i} - \frac{\gamma}{2} - \frac{\eta^2}{2T}}, \quad \nu'_{n_i} = \frac{i\omega_{n_i} + \frac{\gamma}{2} - \frac{\eta^2}{2T}}{i\omega_{n_i} - \frac{\gamma}{2} - \frac{\eta^2}{2T}}. \quad (\text{A28})$$

(Note: Under $\eta = \sqrt{\gamma T}$, the target-mode CE, given by $|\mu'_0|^2$, is unity for any pump with flat intensity $|\beta(t)|^2 = 1/T$ (e.g., all SF pumps).)

For two pump configurations that differ by one frequency-bin index, the corresponding frequency-domain transfer functions are $\tilde{g}_s^{(q)}(l, m) = \mu'_l \delta_{m, l-n-q+1}$, where we write $f(n, m)$ in place of $f(\omega_n, \omega_m)$ when referring to matrix elements, and $q \in \{1, 2\}$ labels the two cases. Thus the time-domain kernel $\mathcal{U}^{(q)}(u, u')$ in Eq. (A22) becomes diagonal in the frequency-bin basis. Explicitly, in the frequency representation, $\tilde{\mathcal{U}}^{(q)} = \text{diag}(|\mu'_{m+n+q-1}|^2)$, since

$$\tilde{\mathcal{U}}^{(q)}(m, m') = \sum_l \tilde{g}_s^{(q)*}(l, m) \tilde{g}_s^{(q)}(l, m') = \sum_l |\mu'_l|^2 \delta_{m, l-n-q+1} \delta_{m', l-n-q+1} = |\mu'_{m+n+q-1}|^2 \delta_{m, m'}. \quad (\text{A29})$$

Each $\tilde{\mathcal{U}}^{(q)}$ is Hermitian and positive semidefinite. After normalization by its trace, $\rho^{(q)} = \tilde{\mathcal{U}}^{(q)} / [\text{Tr } \tilde{\mathcal{U}}^{(q)}]$, it represents a valid mixed state. The indistinguishability between these two mixed states is quantified using the quantum fidelity for mixed states, also known as the Uhlmann fidelity, which reduces to the classical Bhattacharyya form when the two density matrices are diagonal and therefore commute:

$$\mathcal{F}_i(\rho^{(1)}, \rho^{(2)}) = \left(\sum_m \sqrt{\rho^{(1)}(m, m) \rho^{(2)}(m, m)} \right)^2. \quad (\text{A30})$$

Substituting the explicit diagonal elements yields the indistinguishability (fidelity) between the two pump configurations:

$$\mathcal{F}_i = \left(\frac{\sum_k |\mu'_k| |\mu'_{k+1}|}{\sum_k |\mu'_k|^2} \right)^2, \quad (\text{A31})$$

under the natural assumption $\sum_k |\mu'_k|^2 = \sum_k |\mu'_{k+1}|^2$. The dependence of the indistinguishability on $\gamma/\Delta\omega$ is shown in Fig. 5. A high indistinguishability (low sensitivity) indicates that adjacent pump-frequency components produce similar outputs, which directly limits the fidelity achievable for an SF target mode. The fidelity results and the control-mode sensitivity are therefore consistent, together characterizing the gate's spectral sharpness (its ability to resolve nearby pump-frequency components) and its practical mode selectivity.

4. Effect of internal loss

To account for internal losses, we model the coupling to an ancillary bath mode \hat{d}^{in} with loss rate ι . In this case, Eq. (A10) becomes

$$\dot{\hat{b}}(t) = -\frac{\gamma}{2} \hat{b}(t) - \frac{\iota}{2} \hat{b}(t) - \eta \hat{a}_s^{\text{in}}(t) \beta(t) - \frac{\eta^2}{2} \hat{b}(t) |\beta(t)|^2 - \sqrt{\gamma} \hat{a}_i^{\text{in}}(t) - \sqrt{\iota} \hat{d}^{\text{in}}(t). \quad (\text{A32})$$

Applying the same method used for solving Eq. (A10) in the preceding section, and taking the limit $\eta \sim \sqrt{(\gamma + \iota)T} \rightarrow 0$, the idler output in the frequency domain is found to be

$$\hat{a}_i^{\text{out}}(\omega_{n_i}) = \begin{cases} \mu_0'' \hat{A}_s^{\text{in}}(0) + \nu_0'' \hat{a}_i^{\text{in}}(\omega_0) + v_0'' \hat{d}^{\text{in}}(\omega_0), & n_i = 0, \\ \hat{a}_i^{\text{in}}(\omega_{n_i}), & n_i \neq 0, \end{cases} \quad (\text{A33})$$

with coefficients

$$\mu_0'' = -\frac{2\eta\sqrt{\gamma T}}{\gamma T + \iota T + \eta^2}, \quad (\text{A34})$$

$$\nu_0'' = \frac{\eta^2 - \gamma T + \iota T}{\gamma T + \iota T + \eta^2}, \quad (\text{A35})$$

$$v_0'' = -\frac{2\sqrt{\gamma\iota}}{\gamma T + \iota T + \eta^2}. \quad (\text{A36})$$

The CE of the target TM, $|\mu_0''|^2$, reaches its maximum value $1/(1+\iota/\gamma)$, when $\eta = \sqrt{(\gamma + \iota)T}$.

Appendix B: Extension to the $M \times N$ gate

The $M \times N$ gate, based on the CSFG process, is governed by the Hamiltonian

$$\begin{aligned} \hat{H}/\hbar = & \sum_m \omega_{i,c,m} \hat{b}_m^\dagger \hat{b}_m + \sum_{n_s} (\omega_{n_s} + \omega_{s,c}) \hat{a}_s^\dagger(\omega_{n_s}) \hat{a}_s(\omega_{n_s}) \\ & + \sum_{m,n_i} (\omega_{n_i} + \omega_{i,c,m}) \hat{a}_{i,m}^\dagger(\omega_{n_i}) \hat{a}_{i,m}(\omega_{n_i}) \\ & + i\sqrt{\gamma} \left(\sum_m \hat{a}_{i,m}^\dagger \sum_{m'} \hat{b}_{m'} - \sum_{m'} \hat{b}_{m'}^\dagger \sum_m \hat{a}_{i,m} \right) \\ & - i\eta \left[\hat{a}_s \sum_m \hat{b}_m^\dagger \sum_{m'} \beta_{m'}(t) e^{-i\omega_{p,c,m'} t} - \hat{a}_s^\dagger \sum_m \hat{b}_m \sum_{m'} \beta_{m'}^*(t) e^{i\omega_{p,c,m'} t} \right]. \end{aligned} \quad (\text{B1})$$

Here $\omega_{i,c,m} = \omega_{i,c} + m\Omega_{\text{FSR}}$ and $\omega_{p,c,m} = \omega_{p,c} + m\Omega_{\text{FSR}}$. The operator $\hat{a}_{i,m} = \sqrt{1/T} \sum_{n_i} \hat{a}_{i,m}(\omega_{n_i})$ denotes the external idler mode, restricted to one FSR around $\omega_{i,c,m}$ and coupled to intra-cavity mode \hat{b}_m .

In the rotating frame defined by $\hat{a}_s(\omega_{n_s}) \rightarrow \hat{a}_s(\omega_{n_s}) e^{-i\omega_{s,c} t}$, $\hat{a}_{i,m}(\omega_{n_i}) \rightarrow \hat{a}_{i,m}(\omega_{n_i}) e^{-i\omega_{i,c,m} t}$, and $\hat{b}_m \rightarrow \hat{b}_m e^{-i\omega_{i,c,m} t}$, the Langevin equations for the cavity modes become [79]

$$\dot{\hat{b}}_k(t) = -\frac{\gamma}{2} \hat{b}_k(t) - \eta \hat{a}_s^{\text{in}}(t) \beta_k(t) - \frac{\eta^2}{2} \sum_m \hat{b}_m(t) \beta_m^*(t) \beta_k(t) - \sqrt{\gamma} \hat{a}_{i,k}^{\text{in}}(t), \quad (\text{B2})$$

where rapidly rotating terms proportional to $e^{-im\Omega_{\text{FSR}}t}$ ($m \neq 0$) have been neglected.

Solving Eq. (B2) in the limit $\eta \sim \sqrt{\gamma T} \rightarrow 0$ ($\gamma/\Delta\omega \rightarrow 0$) yields the analog of Eq. (A17):

$$\hat{b}_k(t) = -\frac{2}{\gamma T + \eta^2} [\eta \hat{A}_{s,k}^{\text{in}}(0) + \sqrt{\gamma T} \hat{a}_{i,k}^{\text{in}}(\omega_0)] + K_k, \quad (\text{B3})$$

where $\hat{A}_{s,k}^{\text{in}}(0) = \int_{-T/2}^{T/2} dt' \beta_k(t') \hat{a}_s^{\text{in}}(t') = \sum_{n_s} \beta_k(\omega_{-n_s}) \hat{a}_s^{\text{in}}(\omega_{n_s})$, and $K_k \propto \int_{-T/2}^{T/2} dt' \sum_{m \neq k} \hat{b}_m(t') \beta_m^*(t') \beta_k(t')$.

Because the right-hand side of Eq. (B3) is time independent, only the zero-frequency component survives: $\hat{b}_m(\omega_{n_i}) = 0$ for $n_i \neq 0$, as in Eq. (A18). Thus $\hat{b}_m(t) = (1/\sqrt{T}) \sum_{n_i} \hat{b}_m(\omega_{n_i}) \exp(-i\omega_{n_i} t) = (1/\sqrt{T}) \hat{b}_m(\omega_0)$, and

$$K_k \propto \int_{-T/2}^{T/2} dt' \sum_{m \neq k} \hat{b}_m(\omega_0) \beta_m^*(t') \beta_k(t') = \sum_{m \neq k} \hat{b}_m(\omega_0) \delta_{mk} = 0,$$

where we have used the orthogonality of the set $\{\beta_m(t)\}$.

Using the cavity input–output relation

$$\hat{a}_{i,k}^{\text{out}}(t) - \hat{a}_{i,k}^{\text{in}}(t) = \sqrt{\gamma} \hat{b}_k(t), \quad (\text{B4})$$

the idler output field in the k th cavity-resonance channel can be written in the frequency-bin basis as

$$\hat{a}_{i,k}^{\text{out}}(\omega_{n_i}) = \begin{cases} -\frac{1}{\gamma T + \eta^2} [2\eta\sqrt{\gamma T} \hat{A}_{s,k}^{\text{in}}(0) + (\gamma T - \eta^2) \hat{a}_{i,k}^{\text{in}}(\omega_0)], & n_i = 0, \\ \hat{a}_{i,k}^{\text{in}}(\omega_{n_i}), & n_i \neq 0. \end{cases} \quad (\text{B5})$$

In the special case $\eta = \sqrt{\gamma T}$, the outputs simplify to

$$\hat{a}_{i,k}^{\text{out}}(\omega_{n_i}) = \begin{cases} -\hat{A}_{s,k}^{\text{in}}(0), & n_i = 0, \\ \hat{a}_{i,k}^{\text{in}}(\omega_{n_i}), & n_i \neq 0. \end{cases} \quad (\text{B6})$$

This implements an $M \times N$ truncated-unitary (or unitary when $M = N$) operation on the frequency-bin modes [51], with idler output

$$\hat{a}_{i,m}^{\text{out}}(\omega_0) = \sum_l U_{ml} \hat{a}_s^{\text{in}}(\omega_l), \quad U_{ml} = -\beta_m(\omega_{-l}).$$

1. Fidelity and conversion efficiency of the $M \times N$ gate

Define the M -component vectors

$$\vec{b}(t) = \begin{pmatrix} \hat{b}_{+(M-1)/2}(t) \\ \vdots \\ \hat{b}_k(t) \\ \vdots \\ \hat{b}_{-(M-1)/2}(t) \end{pmatrix}, \quad (\vec{a}_i^{\text{in(out)}}(t))_k = \hat{a}_{i,k}^{\text{in(out)}}(t), \quad \vec{f}_s(t) = \hat{a}_s^{\text{in}}(t) \vec{\beta}(t),$$

where $\vec{\beta}(t) = \{\beta_k(t)\}^T$. With these definitions, the coupled equations of motion [Eqs. (B2)] can be written in the compact form

$$\dot{\vec{b}}(t) = -\mathbb{M}(t) \vec{b}(t) - \vec{d}(t), \quad (\text{B7})$$

subject to the boundary condition $\vec{b}(T/2) = \vec{b}(-T/2)$. Here

$$\mathbb{M}(t) \equiv \frac{\gamma}{2} \mathbb{I} + \frac{\eta^2}{2} \mathbb{J}(t), \quad \vec{d}(t) \equiv \sqrt{\gamma} \vec{a}_i^{\text{in}}(t) + \eta \vec{f}_s(t),$$

where \mathbb{I} is the $M \times M$ identity matrix and $\mathbb{J}_{km}(t) = \beta_m^*(t) \beta_k(t)$.

Eq. (B7) is a first-order linear differential equation with time-dependent coefficients. Its exact solution on $[-T/2, T/2]$ can be written as

$$\vec{b}(t) = \int_{-T/2}^{T/2} du \mathbb{K}(t, u) \vec{d}(u),$$

where

$$\mathbb{K}(t, u) = -\mathbb{P}\left(t, -\frac{T}{2}\right) \left[\mathbb{I} - \mathbb{P}\left(\frac{T}{2}, -\frac{T}{2}\right) \right]^{-1} \mathbb{P}\left(\frac{T}{2}, u\right) - \Theta(t - u) \mathbb{P}(t, u).$$

Here the propagator is

$$\mathbb{P}(t, t_0) = \mathcal{T} \exp \left[- \int_{t_0}^t ds \mathbb{M}(s) \right],$$

with \mathcal{T} denoting time ordering.

Using the cavity input–output relation in Eq. (B4), the idler output can be written in the input–output form

$$\vec{a}_i^{\text{out}}(t) = \int_{-T/2}^{T/2} du \vec{G}_s(t, u) \hat{a}_s^{\text{in}}(u) + \int_{-T/2}^{T/2} du \mathbb{G}_i(t, u) \vec{a}_i^{\text{in}}(u), \quad (\text{B8})$$

where

$$\vec{G}_s(t, u) = \sqrt{\gamma} \eta \mathbb{K}(t, u) \vec{\beta}(u), \quad \mathbb{G}_i(t, u) = \gamma \mathbb{K}(t, u) + \delta(t - u) \mathbb{I}.$$

Similar to the $1 \times N$ -gate case, we evaluate the detection-associated fidelity and CE of the $M \times N$ gate. We assume that each output channel is measured by an individual photon counter. The single-channel PC fidelity in Eq. (A23) extends to the multi-channel case in a classical way as

$$\mathcal{F}_i^{\text{PC}} = \frac{\int_{-T/2}^{T/2} dt \left\| \int_{-T/2}^{T/2} du (\vec{\beta}^*(u) \circ \vec{G}_s(t, u)) \right\|_2^2}{\left[\iint_{-T/2}^{T/2} dt du |\vec{G}_s(t, u)|^{\circ 2} \right] \cdot \left[\int_{-T/2}^{T/2} du |\vec{\beta}(u)|^{\circ 2} \right]} = \frac{\int_{-T/2}^{T/2} dt \left\| \int_{-T/2}^{T/2} du (\vec{\beta}^*(u) \circ \vec{G}_s(t, u)) \right\|_2^2}{\iint_{-T/2}^{T/2} dt du |\vec{G}_s(t, u)|^{\circ 2}}. \quad (\text{B9})$$

Here \circ denotes the Hadamard (elementwise) product, and $|X|^{\circ 2}$ denotes elementwise modulus squared, i.e. $|X|^{\circ 2} = (|X_1|^2, \dots, |X_m|^2)$. The norm $\|\cdot\|_2$ is the Euclidean norm, $\|x\|_2 = \sqrt{x^\dagger x}$. Because each channel is detected independently, PC discards all relative phase information between channels, consistent with the invariance of the kernel \mathcal{U} in Eq. (A22) under channel-dependent phase shifts. The corresponding PC-based CE is given by

$$\mathcal{C}_e^{\text{PC}} = \frac{1}{M} \int_{-T/2}^{T/2} dt \left\| \int_{-T/2}^{T/2} du (\vec{\beta}^*(u) \circ \vec{G}_s(t, u)) \right\|_2^2. \quad (\text{B10})$$

If each output channel is instead measured by HD, with the field projected onto the TM $1/\sqrt{T}$ (taken to be the optimal projection for simplicity) and only the zero-frequency component retained, then the measurement yields

$$\vec{A} = \int_{-T/2}^{T/2} \frac{dt}{\sqrt{T}} \vec{a}_i^{\text{out}}(t) = \int_{-T/2}^{T/2} du \vec{\mathcal{H}}(u) \hat{a}_s^{\text{in}}(u),$$

where $\vec{\mathcal{H}}(u) = \int_{-T/2}^{T/2} (dt/\sqrt{T}) \vec{G}_s(t, u)$, and we omit the trivial idler–input vacuum term. The ideal transformation corresponds to $\vec{\mathcal{H}}^{\text{ideal}}(u) = \vec{\beta}(u)$. The associated HD fidelity is defined as the Hilbert–Schmidt overlap between the two kernels,

$$\mathcal{F}_i^{\text{HD}} = \frac{|\text{Tr}(\vec{\mathcal{H}}^\dagger \vec{\mathcal{H}}^{\text{ideal}})|^2}{\text{Tr}(\vec{\mathcal{H}}^\dagger \vec{\mathcal{H}}) \text{Tr}(\vec{\mathcal{H}}^{\text{ideal}\dagger} \vec{\mathcal{H}}^{\text{ideal}})} = \frac{\left| \int_{-T/2}^{T/2} dt \int_{-T/2}^{T/2} du \vec{\beta}^\dagger(u) \vec{G}_s(t, u) \right|^2}{M \int_{-T/2}^{T/2} du \left\| \int_{-T/2}^{T/2} dt \vec{G}_s(t, u) \right\|_2^2}. \quad (\text{B11})$$

where we have used $\int_{-T/2}^{T/2} du \|\vec{\beta}(u)\|_2^2 = M$. The corresponding HD-based CE is

$$\mathcal{C}_e^{\text{HD}} = \frac{|\text{Tr}(\vec{\mathcal{H}}^\dagger \vec{\mathcal{H}}^{\text{ideal}})|^2}{[\text{Tr}(\vec{\mathcal{H}}^{\text{ideal}\dagger} \vec{\mathcal{H}}^{\text{ideal}})]^2} = \frac{1}{M^2 T} \left| \int_{-T/2}^{T/2} dt \int_{-T/2}^{T/2} du \vec{\beta}^\dagger(u) \vec{G}_s(t, u) \right|^2. \quad (\text{B12})$$

From Eqs. (B10) and (B12), we find that the HD-based CE is always less than or equal to the PC-based CE, as guaranteed by the Cauchy–Schwarz inequality. Intuitively, HD projects each output channel onto a single TM and discards all orthogonal components, so any mode mismatch appears as loss in the measured mode, reducing the inferred CE relative to PC.

- [1] M. Luo and X. Wang, Universal quantum computation with qudits, *Science China Physics, Mechanics & Astronomy* **57**, 1712–1717 (2014).
- [2] Y. Wang, Z. Hu, B. C. Sanders, and S. Kais, Qudits and high-dimensional quantum computing, *Frontiers in Physics* **8**, 589504 (2020).
- [3] H.-H. Lu, Z. Hu, M. S. Alshaykh, A. J. Moore, Y. Wang, P. Imany, A. M. Weiner, and S. Kais, Quantum phase estimation with time-frequency qudits in a single photon, *Advanced Quantum Technologies* **3**, 1900074 (2020).
- [4] T. Ralph, K. Resch, and A. Gilchrist, Efficient toffoli gates using qudits, *Physical Review A—Atomic, Molecular, and Optical Physics* **75**, 022313 (2007).
- [5] B. Li, Z.-H. Yu, and S.-M. Fei, Geometry of quantum computation with qutrits, *Scientific reports* **3**, 2594 (2013).
- [6] B. P. Lanyon, M. Barbieri, M. P. Almeida, T. Jennewein, T. C. Ralph, K. J. Resch, G. J. Pryde, J. L. O’Brien, A. Gilchrist, and A. G. White, Simplifying quantum logic using higher-dimensional hilbert spaces, *Nature Physics* **5**, 134–140 (2008).
- [7] W.-Q. Liu and H.-R. Wei, Optimal synthesis of the fredkin gate in a multilevel system, *New Journal of Physics* **22**, 063026 (2020).
- [8] A. Bocharov, M. Roetteler, and K. M. Svore, Factoring with qutrits: Shor’s algorithm on ternary and metaplectic quantum architectures, *Physical Review A* **96**, 012306 (2017).
- [9] A. Babazadeh, M. Erhard, F. Wang, M. Malik, R. Nouroozi, M. Krenn, and A. Zeilinger, High-dimensional single-photon quantum gates: concepts and experiments, *Physical review letters* **119**, 180510 (2017).
- [10] S. Muralidharan, C.-L. Zou, L. Li, J. Wen, and L. Jiang, Overcoming erasure errors with multilevel systems, *New Journal of Physics* **19**, 013026 (2017).
- [11] E. T. Campbell, Enhanced fault-tolerant quantum computing in d-level systems, *Physical review letters* **113**, 230501 (2014).

- [12] M. Howard and E. Campbell, Application of a resource theory for magic states to fault-tolerant quantum computing, *Physical review letters* **118**, 090501 (2017).
- [13] E. T. Campbell, H. Anwar, and D. E. Browne, Magic-state distillation in all prime dimensions using quantum reed-muller codes, *Physical Review X* **2**, 041021 (2012).
- [14] N. C. Menicucci, P. Van Loock, M. Gu, C. Weedbrook, . f. T. C. Ralph, and M. A. Nielsen, Universal quantum computation with continuous-variable cluster states, *Physical review letters* **97**, 110501 (2006).
- [15] M. Gu, C. Weedbrook, N. C. Menicucci, T. C. Ralph, and P. Van Loock, Quantum computing with continuous-variable clusters, *Physical Review A—Atomic, Molecular, and Optical Physics* **79**, 062318 (2009).
- [16] M. H. S. Amin, N. G. Dickson, and P. Smith, Adiabatic quantum optimization with qudits, *Quantum Information Processing* **12**, 1819–1829 (2012).
- [17] H. Bechmann-Pasquinucci and W. Tittel, Quantum cryptography using larger alphabets, *Physical Review A* **61**, 062308 (2000).
- [18] J. Cortese, Holevo-schumacher-westmoreland channel capacity for a class of qudit unital channels, *Physical Review A* **69**, 022302 (2004).
- [19] P. B. Dixon, G. A. Howland, J. Schneeloch, and J. C. Howell, Quantum mutual information capacity for high-dimensional entangled states, *Physical review letters* **108**, 143603 (2012).
- [20] X.-M. Hu, Y. Guo, B.-H. Liu, Y.-F. Huang, C.-F. Li, and G.-C. Guo, Beating the channel capacity limit for superdense coding with entangled ququarts, *Science advances* **4**, eaat9304 (2018).
- [21] X.-L. Wang, X.-D. Cai, Z.-E. Su, M.-C. Chen, D. Wu, L. Li, N.-L. Liu, C.-Y. Lu, and J.-W. Pan, Quantum teleportation of multiple degrees of freedom of a single photon, *Nature* **518**, 516–519 (2015).
- [22] S. Hao, H. Shi, W. Li, J. H. Shapiro, Q. Zhuang, and Z. Zhang, Entanglement-assisted communication surpassing the ultimate classical capacity, *Phys. Rev. Lett.* **126**, 250501 (2021).
- [23] D.-S. Ding, W. Zhang, S. Shi, Z.-Y. Zhou, Y. Li, B.-S. Shi, and G.-C. Guo, High-dimensional entanglement between distant atomic-ensemble memories, *Light: Science & Applications* **5**, e16157–e16157 (2016).
- [24] V. Parigi, V. D’Ambrosio, C. Arnold, L. Marrucci, F. Sciarrino, and J. Laurat, Storage and retrieval of vector beams of light in a multiple-degree-of-freedom quantum memory, *Nature*

communications **6**, 7706 (2015).

[25] M. Dąbrowski, M. Mazelanik, M. Parniak, A. Leszczyński, M. Lipka, and W. Wasilewski, Certification of high-dimensional entanglement and einstein-podolsky-rosen steering with cold atomic quantum memory, *Physical Review A* **98**, 042126 (2018).

[26] N. J. Cerf, M. Bourennane, A. Karlsson, and N. Gisin, Security of quantum key distribution using d-level systems, *Physical review letters* **88**, 127902 (2002).

[27] F. Bouchard, R. Fickler, R. W. Boyd, and E. Karimi, High-dimensional quantum cloning and applications to quantum hacking, *Science advances* **3**, e1601915 (2017).

[28] N. T. Islam, C. C. W. Lim, C. Cahall, J. Kim, and D. J. Gauthier, Provably secure and high-rate quantum key distribution with time-bin qudits, *Science advances* **3**, e1701491 (2017).

[29] S. Aaronson and A. Arkhipov, The computational complexity of linear optics, in *Proceedings of the forty-third annual ACM symposium on Theory of computing* (2011) pp. 333–342.

[30] C. S. Hamilton, R. Kruse, L. Sansoni, S. Barkhofen, C. Silberhorn, and I. Jex, Gaussian boson sampling, *Physical review letters* **119**, 170501 (2017).

[31] M. Neeley, M. Ansmann, R. C. Bialczak, M. Hofheinz, E. Lucero, A. D. O’Connell, D. Sank, H. Wang, J. Wenner, A. N. Cleland, *et al.*, Emulation of a quantum spin with a superconducting phase qudit, *Science* **325**, 722 (2009).

[32] S. Lloyd, Enhanced sensitivity of photodetection via quantum illumination, *Science* **321**, 1463 (2008).

[33] X. Chen and Z. Ye, Quantum illumination via correlation-to-displacement conversion with cavity-enhanced mode selection, *Opt. Express* **33**, 32374 (2025).

[34] H. Shi, B. Zhang, J. H. Shapiro, Z. Zhang, and Q. Zhuang, Optimal entanglement-assisted electromagnetic sensing and communication in the presence of noise, *Phys. Rev. Appl.* **21**, 034004 (2024).

[35] D. Collins, N. Gisin, N. Linden, S. Massar, and S. Popescu, Bell inequalities for arbitrarily high-dimensional systems, *Physical review letters* **88**, 040404 (2002).

[36] T. Vértesi, S. Pironio, and N. Brunner, Closing the detection loophole in bell experiments using qudits, *Physical review letters* **104**, 060401 (2010).

[37] A. C. Dada, J. Leach, G. S. Buller, M. J. Padgett, and E. Andersson, Experimental high-dimensional two-photon entanglement and violations of generalized bell inequalities, *Nature Physics* **7**, 677 (2011).

[38] H.-S. Zhong, H. Wang, Y.-H. Deng, M.-C. Chen, L.-C. Peng, Y.-H. Luo, J. Qin, D. Wu, X. Ding, Y. Hu, *et al.*, Quantum computational advantage using photons, *Science* **370**, 1460 (2020).

[39] J. Carolan, C. Harrold, C. Sparrow, E. Martín-López, N. J. Russell, J. W. Silverstone, P. J. Shadbolt, N. Matsuda, M. Oguma, M. Itoh, *et al.*, Universal linear optics, *Science* **349**, 711 (2015).

[40] L. S. Madsen, F. Laudenbach, M. F. Askarani, F. Rortais, T. Vincent, J. F. Bulmer, F. M. Miatto, L. Neuhaus, L. G. Helt, M. J. Collins, *et al.*, Quantum computational advantage with a programmable photonic processor, *Nature* **606**, 75 (2022).

[41] J. M. Lukens and P. Lougovski, Frequency-encoded photonic qubits for scalable quantum information processing, *Optica* **4**, 8 (2017).

[42] H.-H. Lu, J. M. Lukens, B. P. Williams, P. Imany, N. A. Peters, A. M. Weiner, and P. Lougovski, A controlled-not gate for frequency-bin qubits, *npj Quantum Information* **5**, 24 (2019).

[43] H.-H. Lu, J. M. Lukens, N. A. Peters, O. D. Odele, D. E. Leaird, A. M. Weiner, and P. Lougovski, Electro-optic frequency beam splitters and tritters for high-fidelity photonic quantum information processing, *Phys. Rev. Lett.* **120**, 030502 (2018).

[44] H.-H. Lu, J. M. Lukens, N. A. Peters, B. P. Williams, A. M. Weiner, and P. Lougovski, Quantum interference and correlation control of frequency-bin qubits, *Optica* **5**, 1455 (2018).

[45] H.-H. Lu, E. M. Simmerman, P. Lougovski, A. M. Weiner, and J. M. Lukens, Fully arbitrary control of frequency-bin qubits, *Phys. Rev. Lett.* **125**, 120503 (2020).

[46] H.-H. Lu, M. Liscidini, A. L. Gaeta, A. M. Weiner, and J. M. Lukens, Frequency-bin photonic quantum information, *Optica* **10**, 1655 (2023).

[47] H.-H. Lu, K. V. Myilswamy, R. S. Bennink, S. Seshadri, M. S. Alshaykh, J. Liu, T. J. Kippenberg, D. E. Leaird, A. M. Weiner, and J. M. Lukens, Bayesian tomography of high-dimensional on-chip biphoton frequency combs with randomized measurements, *Nature Communications* **13**, 4338 (2022).

[48] S. Seshadri, H.-H. Lu, D. E. Leaird, A. M. Weiner, and J. M. Lukens, Complete frequency-bin bell basis synthesizer, *Phys. Rev. Lett.* **129**, 230505 (2022).

[49] N. B. Lingaraju, H.-H. Lu, D. E. Leaird, S. Estrella, J. M. Lukens, and A. M. Weiner, Bell state analyzer for spectrally distinct photons, *Optica* **9**, 280 (2022).

[50] L. Serino, J. Gil-Lopez, M. Stefszky, R. Ricken, C. Eigner, B. Brecht, and C. Silberhorn,

Realization of a multi-output quantum pulse gate for decoding high-dimensional temporal modes of single-photon states, PRX Quantum **4**, 020306 (2023).

[51] P. Folge, M. Stefszky, B. Brecht, and C. Silberhorn, A framework for fully programmable frequency-encoded quantum networks harnessing multioutput quantum pulse gates, PRX Quantum **5**, 040329 (2024).

[52] S. De, V. Ansari, J. Sperling, S. Barkhofen, B. Brecht, and C. Silberhorn, Realization of high-fidelity unitary operations on up to 64 frequency bins, Phys. Rev. Res. **6**, L022040 (2024).

[53] A. Eckstein, B. Brecht, and C. Silberhorn, A quantum pulse gate based on spectrally engineered sum frequency generation, Opt. Express **19**, 13770 (2011).

[54] B. Brecht, A. Eckstein, R. Ricken, V. Quiring, H. Suche, L. Sansoni, and C. Silberhorn, Demonstration of coherent time-frequency schmidt mode selection using dispersion-engineered frequency conversion, Phys. Rev. A **90**, 030302 (2014).

[55] D. V. Reddy, M. G. Raymer, C. J. McKinstrie, L. Mejling, and K. Rottwitt, Temporal mode selectivity by frequency conversion in second-order nonlinear optical waveguides, Opt. Express **21**, 13840 (2013).

[56] D. V. Reddy, M. G. Raymer, and C. J. McKinstrie, Efficient sorting of quantum-optical wave packets by temporal-mode interferometry, Opt. Lett. **39**, 2924 (2014).

[57] D. V. Reddy and M. G. Raymer, High-selectivity quantum pulse gating of photonic temporal modes using all-optical ramsey interferometry, Optica **5**, 423 (2018).

[58] M. G. Raymer and I. A. Walmsley, Temporal modes in quantum optics: then and now, Physica Scripta **95**, 064002 (2020).

[59] B. Brecht, D. V. Reddy, C. Silberhorn, and M. G. Raymer, Photon temporal modes: A complete framework for quantum information science, Phys. Rev. X **5**, 041017 (2015).

[60] Z. Ou, *Quantum Optics for Experimentalists* (World Scientific, 2017).

[61] This corresponds to the regime in which the phase-matching factor $C = \int_0^L e^{i\Delta kz} dz$ in \hat{H}_1 can be treated as a constant. This is valid when the cavity linewidth and pump bandwidth restrict the interaction to frequency components satisfying $\Delta kL \ll 1$ (typically $\sim 10^{-2}$), so that off-phase-matched terms are strongly suppressed. Here Δk is the phase mismatch and L is the nonlinear interaction length [33, 62].

[62] See Supplemental Material.

[63] R. Ikuta, R. Tani, M. Ishizaki, S. Miki, M. Yabuno, H. Terai, N. Imoto, and T. Yamamoto,

Frequency-multiplexed photon pairs over 1000 modes from a quadratic nonlinear optical waveguide resonator with a singly resonant configuration, *Physical review letters* **123**, 193603 (2019).

[64] M. Kues, C. Reimer, J. M. Lukens, W. J. Munro, A. M. Weiner, D. J. Moss, and R. Morandotti, Quantum optical microcombs, *Nature Photonics* **13**, 170 (2019).

[65] J. A. Jaramillo-Villegas, P. Imany, O. D. Odele, D. E. Leaird, Z.-Y. Ou, M. Qi, and A. M. Weiner, Persistent energy–time entanglement covering multiple resonances of an on-chip biphoton frequency comb, *Optica* **4**, 655 (2017).

[66] X. Chen and Q. Zhuang, Entanglement-assisted detection of fading targets via correlation-to-displacement conversion, *Phys. Rev. A* **107**, 062405 (2023).

[67] M. Reichert, Q. Zhuang, J. H. Shapiro, and R. Di Candia, Quantum illumination with a hetero-homodyne receiver and sequential detection, *Phys. Rev. Appl.* **20**, 014030 (2023).

[68] J. Angeletti, H. Shi, T. Lakshmanan, D. Vitali, and Q. Zhuang, Microwave quantum illumination with correlation-to-displacement conversion, *Phys. Rev. Appl.* **20**, 024030 (2023).

[69] N. Sangouard, C. Simon, H. De Riedmatten, and N. Gisin, Quantum repeaters based on atomic ensembles and linear optics, *Reviews of Modern Physics* **83**, 33 (2011).

[70] T. Chakraborty, A. Das, H. van Brug, O. Pietx-Casas, P.-C. Wang, G. C. d. Amaral, A. L. Tchebotareva, and W. Tittel, Towards a spectrally multiplexed quantum repeater, *npj Quantum Information* **11**, 3 (2025).

[71] N. Sinclair, E. Saglamyurek, H. Mallahzadeh, J. A. Slater, M. George, R. Ricken, M. P. Hedges, D. Oblak, C. Simon, W. Sohler, *et al.*, Spectral multiplexing for scalable quantum photonics using an atomic frequency comb quantum memory and feed-forward control, *Physical review letters* **113**, 053603 (2014).

[72] D.-S. Ding, W. Zhang, S. Shi, Z.-Y. Zhou, Y. Li, B.-S. Shi, and G.-C. Guo, High-dimensional entanglement between distant atomic-ensemble memories, *Light: Science & Applications* **5**, e16157 (2016).

[73] A. Khodadad Kashi and M. Kues, Frequency-bin-encoded entanglement-based quantum key distribution in a reconfigurable frequency-multiplexed network, *Light: Science & Applications* **14**, 49 (2025).

[74] E. Knill, R. Laflamme, and G. J. Milburn, A scheme for efficient quantum computation with linear optics, *nature* **409**, 46 (2001).

[75] S. Paesani, J. F. Bulmer, A. E. Jones, R. Santagati, and A. Laing, Scheme for universal high-

dimensional quantum computation with linear optics, *Physical Review Letters* **126**, 230504 (2021).

- [76] Z. Ou, *Multi-Photon Quantum Interference* (Springer US, 2007).
- [77] Z. Bai, Z. Zhao, M. Tian, D. Jin, Y. Pang, S. Li, X. Yan, Y. Wang, and Z. Lu, A comprehensive review on the development and applications of narrow-linewidth lasers, *Microwave and Optical Technology Letters* **64**, 2244 (2022).
- [78] C. W. Gardiner and M. J. Collett, Input and output in damped quantum systems: Quantum stochastic differential equations and the master equation, *Phys. Rev. A* **31**, 3761 (1985).
- [79] L. Knöll, W. Vogel, and D.-G. Welsch, Resonators in quantum optics: A first-principles approach, *Phys. Rev. A* **43**, 543 (1991).